Electrical Reservoirs for Bilayer Excitons

Ming Xie and A. H. MacDonald

Phys. Rev. Lett. **121**, 067702 — Published 8 August 2018

DOI: 10.1103/PhysRevLett.121.067702

Electrical Reservoirs for Bilayer Excitons

Ming Xie and A. H. MacDonald
Department of Physics, The University of Texas at Austin, Austin, TX 78712, USA
(Dated: July 23, 2018)

The ground state of two-dimensional (2D) electron systems with equal low densities of electrons and holes in nearby layers is an exciton fluid. We show that a reservoir for excitons can be established by contacting the two layers separately and maintaining the chemical potential difference at a value less than the spatially indirect band gap, thereby avoiding the presence of free carriers in either layer. Equilibration between the exciton fluid and the contacts proceeds via a process involving virtual intermediate states in which an unpaired electron or hole virtually occupies a free carrier state in one of the 2D layers. We derive an approximate relationship between the exciton-contact equilibration rate and the electrical conductances between the contacts and individual 2D layers when the contact chemical potentials align with the free-carrier bands, and explain how electrical measurements can be used to measure thermodynamic properties of the exciton fluids.

PACS numbers: 71.35.-y, 73.21.-b

Introduction.—Excitons are composite bosonic particles in which conduction band electrons bind with valence band holes. Excitons normally exist as excited states of semiconductors and insulators, and can have extremely long lifetimes when the electron and hole are separated in momentum-space, or in real-space [1], or both. Bose-Einstein condensation of long-lived excitons was predicted several decades ago [2], and is thought to have been realized relatively recently in semiconductor quantum well [3–7] double-layers. Closely related polariton condensate states, in which longer range coherence is assisted by the small masses of 2D vertical cavity photons, are regularly realized and have been studied extensively over the past decade [8–18]. In typical exciton-condensation experiments a population of electrons and holes is generated in nearby 2D layers by optical excitation. Free electrons and holes can also be injected electrically if contacts can be established to conduction and valence bands [19–22]. The electrons and holes then combine to form excitons and the excitonic state is revealed by photons emitted during the exciton radiative decay process [23–25]. In this paper we propose and theoretically analyze a mechanism that allows direct electrical control of the chemical potential of spatially indirect exciton fluids without populating free electron and hole states. The mechanism requires substantial exciton binding energies in systems with long electron-hole recombination times. Our proposal is motivated by the properties of van der Waals (vdW) heterojunction systems in which single-layer semiconductors are separated by hexagonal boron nitride (hBN) barrier layers.

In recent years, 2D transition metal dichalcogenide (TMD) semiconductors have been established as an exciting exciton physics platform [26–28] in which energy scales are enhanced by strong Coulomb interactions. Surprising flexibility in the design of optical and electronic properties can be achieved [29–31] by stacking vdW coupled 2D materials in a variety of different arrangements.

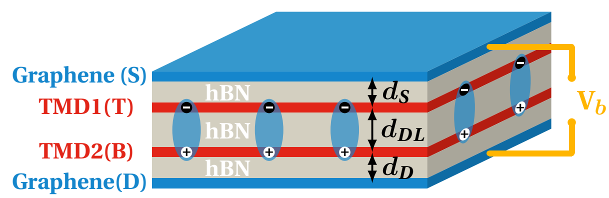

FIG. 1. (Color online) Schematic illustration of a 2D material heterojunction capable of supporting a spatially indirect exciton condensate, and of an electrode pair that can act as a reservoir for spatially indirect excitons.

vdW heterojunctions involving 2D semiconductors can host spatially indirect excitons formed from electrons and holes in two different layers with binding energies that remain large, even when the electron and hole layers are separated by hBN layers that increase exciton lifetimes by orders of magnitude from the nanosecond range [32–34] that applies in the absence of spacer layers.

When the chemical potentials of contact electrodes are inside the energy gaps of the 2D semiconductors, electrons cannot tunnel into double-layer band states. However, because of the Coulomb interaction and the exciton binding energy that it produces, correlated pair tunneling from electrodes connected to the two different layers is possible. In this Letter, we develop a microscopic model of this two-particle tunneling process and argue that it can allow electrode pairs to act directly as exciton reservoirs with a well-defined chemical potential set by the source-to-drain bias. Direct exciton reservoirs have advantages for exciton generation and control over the commonly employed indirect optical and electrical generation processes that start by generating free electrons and holes, and we expect in particular that they will enable electrical measurements of the transport properties of exciton fluids.

Correlated pair tunneling.—We consider the vertically stacked multilayer heterostructure system illustrated in

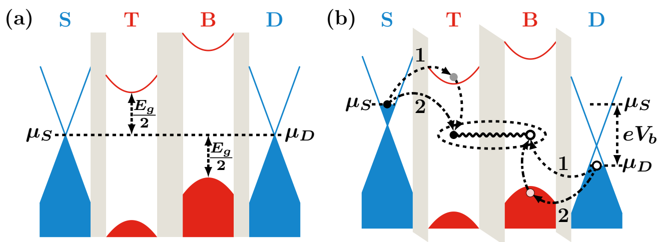

FIG. 2. (Color online) Schematic band diagrams for the vertical vdW heterostructure systems of interest for the case of (a) zero applied bias and (b) a finite bias V_b satisfying indirect gap $E_g > eV_b > \mu^0_{ex}$ where μ^0_{ex} is the energy of an isolated spatially indirect exciton. In case (b), the filled (empty) black circles represents electrons (holes) and the gray (pink) circle represents a virtual state in the T(B) layer. 1 and 2 label two possible tunneling paths as discussed in detail in the text.

Fig. 1, which contains a TMD semiconductor double-layer (DL) with a hBN barrier layer sufficiently thick to suppress tunneling, and source (S) and drain (D) electrodes that contact the two layers separately. For the sake of definiteness we have assumed that the electrodes are formed from graphene sheets instead of metals since these have less influence on exciton binding energies [35], but this detail is inessential. Dynamic screening due to source-drain electron-hole pair excitations is negligible because of the suppression of source-to-drain tunneling by the tunnel barrier. We also assume that the top (T) layer and bottom (B) layer materials are chosen so that the conduction band minimum and valence band maximum are respectively above and below but close to the graphene sheet Dirac point (for example, T=MoS_2 and B=WSe_2 [36]) as illustrated in Fig. 2(a). Once the bias voltage between S and D, $\mu_S - \mu_D = eV_b$, exceeds the energy needed to create an isolated indirect exciton, an exciton fluid will form whose equilibrium chemical potential equals eV_b, where $e > 0$. We discuss the equilibration process below.

The total Hamiltonian of the four-layer system is

$$\hat{\mathcal{H}} = \hat{\mathcal{H}}_S + \hat{\mathcal{H}}_D + \hat{\mathcal{H}}_{DL} + \hat{\mathcal{H}}_t. \tag{1}$$

where $\hat{\mathcal{H}}_S$ and $\hat{\mathcal{H}}_D$ are the linear band Hamiltonians of the graphene electrodes, and $\hat{\mathcal{H}}_{DL}$ is the DL Hamiltonian including Coulomb interactions. In this paper we assume that the TMD DL is in its exciton condensate ground state and ignore its spin degree of freedom. Tunneling between the electrodes and the double-layer system is accounted for by

$$\hat{\mathcal{H}}_t = \sum_{\boldsymbol{k},\bar{\boldsymbol{p}}} t^S_{\boldsymbol{k}\bar{\boldsymbol{p}}}\, \hat{c}^\dagger_{\boldsymbol{k},T} \hat{a}_{\bar{\boldsymbol{p}},S} + t^D_{\boldsymbol{k}\bar{\boldsymbol{p}}}\, \hat{c}^\dagger_{\boldsymbol{k},B} \hat{a}_{\bar{\boldsymbol{p}},D} + h.c. \tag{2}$$

where $t^{S(D)}_{\boldsymbol{k}\bar{\boldsymbol{p}}}$ is a tunneling matrix element. $\bar{\boldsymbol{p}} \equiv (\boldsymbol{p}, \lambda, \tau)$ is a compound index that combines the 2D momentum $\boldsymbol{p}$, the band index $\lambda = c, v$ and the valley index τ of the graphene electrode states. In Eq. (2), $\hat{a}$ is the creation operator in the electrodes and $\hat{c}^\dagger_{T(B)}$ is the creation operator for conduction band electrons in T and valence band electrons in B. For single-grain hBN tunnel barriers, the tunneling properties can have very specific momentum dependence which does not play an essential role and is not accounted for below, but is sensitive to the relative orientation of the various 2D material layers [37, 38]. We neglect interlayer tunneling between the T and B primarily because we are interested in a bias voltage regime in which free carriers are not present to tunnel. We also set the interlayer radiative recombination rate to zero in order to focus on double-electrode reservoir properties. In practice we anticipate that the interplay between our exciton reservoirs and interlayer radiative recombination, whose strength can be adjusted over orders of magnitude by varying the thickness and orientation of the hBN barrier layer, opens up a rich range of opto-electronic phenomena for study that are a primary motivation for this work.

The band diagram of the vertical vdW heterostructure system is shown schematically in Fig. 2. At zero bias (Fig. 2(a)), we assume that both graphene electrodes are neutral and that the aligned Dirac points are in the middle of the spatially indirect band gap E_g. When a bias voltage in the subgap regime ($E_g > eV_b > 0$) is applied, tunneling between the electrodes and free-carrier states in the TMD layers is prohibited by energy conservation. (Note that E_g increases with V_b, and that direct tunneling of electrons from source to drain is extremely strongly suppressed because it must navigate three tunneling barriers.) Our interest here is in the bias regime $E_g > V_b > \mu^0_{ex}$, where μ^0_{ex} is the energy of an isolated spatially indirect exciton. In this bias voltage regime energy conservation can be achieved by the two-particle tunneling process illustrated in Fig. 2(b). The state created when an electron from S tunnels to a virtual state in T and a hole from D subsequently tunnels to B has a finite overlap with an exciton fluid state (path 1). An alternative and equally possible path is for a hole from D to tunnel to a virtual state in B first (path 2). Each tunneling process effectively transfers one electron from S to D and creates an exciton in the DL. We concentrate here on the case of $T < T_c$ for which the excitons form a condensate, although the main idea of using an electrode pair as a reservoir for excitons applies equally well when the excitons form a non-condensed gas. For the low temperature case we find that because of the stimulated scattering characteristic of bosonic statistics, a major fraction of the excitons added or removed from the system are simply added or removed from the condensate.

The condensate state of spatially indirect excitons has been extensively studied in previous work [39–41] using a

BCS-like mean field theory approach in which the ground state is found by minimizing $\langle \hat{\mathcal{H}}_{DL} - \mu_{ex}\hat{\mathcal{N}}\rangle$ in the space of Slater determinant states with coherence between conduction and valence bands. Here $\hat{\mathcal{N}} = \sum_{\boldsymbol{k}}(\hat{c}^\dagger_{\boldsymbol{k},T}\hat{c}_{\boldsymbol{k},T} + \hat{c}_{\boldsymbol{k},B}\hat{c}^\dagger_{\boldsymbol{k},B})/2$ is the total number of electron-hole pairs. The mean-field Hamiltonian of the exciton condensate system is

$$\hat{\mathcal{H}}^{MF}_{DL} = E_G + \sum_{\boldsymbol{k}} E_{\boldsymbol{k}}(\hat{\gamma}^\dagger_{\boldsymbol{k},0}\hat{\gamma}_{\boldsymbol{k},0} - \hat{\gamma}^\dagger_{\boldsymbol{k},1}\hat{\gamma}_{\boldsymbol{k},1}) + \mu_{ex}\hat{\mathcal{N}} \quad (3)$$

where E_G is the condensate ground state energy and μ_{ex} the exciton chemical potential. The quasiparticle energy dispersion is $E_{\boldsymbol{k}} = \sqrt{(\epsilon^T_{\boldsymbol{k}} - \mu_{ex}/2)^2 + \Delta^2_{\boldsymbol{k}}}$, where we have assumed that the DL energy dispersion $\epsilon^T_{\boldsymbol{k}} = -\epsilon^B_{\boldsymbol{k}} = \hbar^2k^2/(2m) + E_g/2$ and that the order parameter $\Delta_{\boldsymbol{k}}$ is real. $\hat{\gamma}^\dagger_{\boldsymbol{k},0} = u_{\boldsymbol{k}}\hat{c}^\dagger_{\boldsymbol{k},T} + v_{\boldsymbol{k}}\hat{c}^\dagger_{\boldsymbol{k},B}$ and $\gamma^\dagger_{\boldsymbol{k},1} = v_{\boldsymbol{k}}\hat{c}^\dagger_{\boldsymbol{k},T} - u_{\boldsymbol{k}}\hat{c}^\dagger_{\boldsymbol{k},B}$ are creation operators for states in the empty and occupied dressed quasiparticle bands, respectively, and $u_{\boldsymbol{k}}$ and $v_{\boldsymbol{k}}$ are coherence factors that depend on the pair potential $\Delta_{\boldsymbol{k}}$ which is determined in turn by solving a self-consistent equation that has solutions only if μ_{ex} exceeds μ^0_{ex} [39].

The two-particle tunneling rate can be obtained by applying Fermi's golden rule to the second order tunneling process. We find that the net rate at which excitons are added to the condensate is

$$\frac{dn_{ex}}{dt} = \frac{2\pi}{\hbar A}\sum_{\bar{\boldsymbol{p}},\bar{\boldsymbol{p}}'} |M_{\bar{\boldsymbol{p}}\bar{\boldsymbol{p}}'}|^2 (f^S_{\bar{\boldsymbol{p}}} - f^D_{\bar{\boldsymbol{p}}'})\delta(\epsilon^S_{\bar{\boldsymbol{p}}} - \epsilon^D_{\bar{\boldsymbol{p}}'} - \mu_{ex}) \quad (4)$$

where $f^\alpha_{\bar{\boldsymbol{p}}}$, with $\alpha = S, D$, is the Fermi distribution function. The matrix element in Eq. (4)

$$M_{\bar{\boldsymbol{p}}\bar{\boldsymbol{p}}'} = \sum_{\boldsymbol{k}} u_{\boldsymbol{k}} v_{\boldsymbol{k}} t^S_{\boldsymbol{k}\bar{\boldsymbol{p}}} t^{D*}_{\boldsymbol{k}\bar{\boldsymbol{p}}'} \left\{ \frac{1}{E^0_{\boldsymbol{k}} - \epsilon^S_{\bar{\boldsymbol{p}}}} + \frac{1}{\epsilon^D_{\bar{\boldsymbol{p}}'} - E^1_{\boldsymbol{k}}} \right\} \quad (5)$$

where $E^0_{\boldsymbol{k}} = E_{\boldsymbol{k}} + \mu_{ex}/2$ and $E^1_{\boldsymbol{k}} = -E^0_{\boldsymbol{k}}$ are the energies required to add quasiparticles of momentum $\boldsymbol{k}$ to bands 0 and 1, respectively. The energy denominators account for the finite energy cost of hopping to the intermediate virtual states, and never vanish in the bias voltage range of interest. The two terms in the matrix element account for the two tunneling paths depicted in Fig. 2(b).

The evaluation of $|M_{\bar{\boldsymbol{p}}\bar{\boldsymbol{p}}'}|^2$ in Eq. (5) requires knowledge of the momentum dependent tunneling amplitudes $t^\alpha_{\boldsymbol{k}\bar{\boldsymbol{p}}}$. We simplify our calculation by assuming that interfacial disorder plays an important role in determining the tunneling amplitude. We employ a Gaussian random tunneling model for which $\langle t^\alpha(\boldsymbol{r})\rangle_{\rm dis} = 0$ and the second order correlation functions satisfy

$$\langle t^\alpha(\boldsymbol{r}) t^{\alpha'*}(\boldsymbol{r}')\rangle_{\rm dis} = |\Delta t|^2 \mathcal{F}(\boldsymbol{r} - \boldsymbol{r}')\delta_{\alpha\alpha'}, \quad (6)$$

where $\langle\cdots\rangle_{\rm dis}$ is the disorder average and $\mathcal{F}(\boldsymbol{r} - \boldsymbol{r}')$ is a smoothly decaying function of the distance $|\boldsymbol{r} - \boldsymbol{r}'|$. For

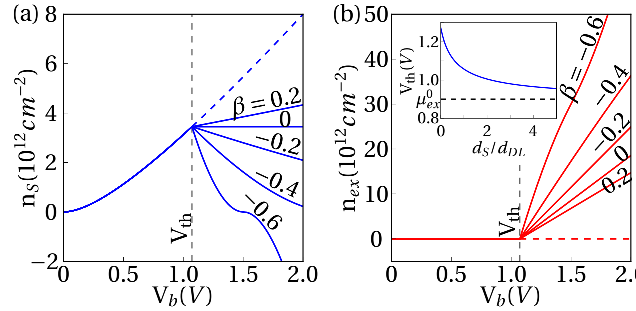

FIG. 3. Equilibrium electrode densities (a) and exciton densities (b) at different values of $\beta = g_{XC}/g_H$, where g_H is fixed with its value set by choosing $d_{DL} = 1nm$. These results were calculated for $d_S = d_D = d_{DL}$ spatially indirect gap $E_g(0) = 1.1eV$, and exciton binding energy $E_b = 0.2eV$. The extended (colored) dashed line represents electrode densities in the case in which the TMD double-layer that hosts excitons is absent. The vertical gray dashed lines indicates the threshold voltage at which the dual electrodes establish a reservoir for excitons. Inset: Threshold voltage as a function of d_S/d_{DL}. The dashed line indicates the zero electrode density limit of the isolated exciton energy μ^0_{ex}.

low exciton densities and $V_b > \mu^0_{ex}$ limit, we obtain the tunneling current-voltage equation

$$I_{ex} \approx G_{ex}(V_b - \mu_{ex}/e). \quad (7)$$

($\mu_{ex} > \mu^0_{ex}$ at finite exciton density.) The effective exciton tunneling conductance G_{ex} is given approximately by

$$G_{ex} = \frac{A g^S_N g^D_N n_{ex} a^2_B}{e^2/\hbar}\frac{8}{\rho_0 E_b}, \quad (8)$$

where g^S_N and g^D_N are the normal tunneling conductances per unit area between S and T and between D and B, respectively, ρ_0 is the density of states of quasiparticle band 0, a_B is the Bohr radius, and E_b the exciton binding energy. The tunneling conductance in Eq. (8) is proportional to the exciton condensate density n_{ex} because of the bosonic stimulated scattering effect. Since the fraction of uncondensed excitons is small in the low density BEC limit, we have assumed in deriving this simple result that the contributions from processes with a final state exciton outside the condensate are negligible. Using the typical values $g^S_N = g^D_N \sim 10^{-2}e^2/h\cdot\mu m^{-2}$, $n_{ex}a^2_B \sim 0.01$, and taking the quasiparticle band masses in the TMD layers close to the bare electron mass, we estimate that G_{ex} is in the order $10^{-11}e^2/h\cdot\mu m^{-2}$.

Eq. (7) states that a time-independent quasi-equilibrium is reached when $eV_b = \mu_{ex}$. We say quasi-equilibrium here, rather than simply equilibrium, to emphasize that we are assuming that excitons cannot annihilate by radiative recombination. As long as all processes in which electrons move between the two TMD layers are absent, we effectively have an equilibrium problem

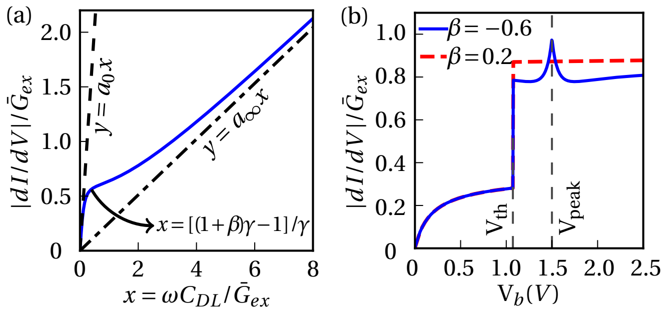

FIG. 4. (Color online) Differential conductance as a function of (a) $x = \omega C_{DL}/\bar{G}_{ex}$ and (b) bias voltage V_b. The dashed line and the dash-dotted line in (a) shows the linear relation at low and high frequency limits, respectively.

in which the spatially indirect band gap is tuned electrically by varying V_b. We do not emphasize this distinction between equilibrium and quasi-equilibrium below.

Electrical characteristics of exciton reservoirs.— Because of repulsive interactions between excitons, their chemical potential increases with exciton density [39–41]. For spatially indirect excitons $\mu_{ex} = \mu^0_{ex}+(g_H+g_{XC})n_{ex}$, where $g_H = e^2/C_{DL} = \epsilon/(4\pi d_{DL})$ and g_{XC} are the Hartree and exchange-correlation contributions to the effective exciton-exciton interaction. The Hartree term accounts for the capacitive coupling between T and B layers, whereas g_{XC}, which is density-dependent and cannot be evaluated exactly, accounts for exchange and correlation effects contributions due to both intralayer and interlayer Coulombic interactions and therefore also depend on the interlayer spacing d_{DL}. When we add the potential energy associated with charged electrodes, the exciton chemical potential in our geometry has an additional electrostatic contribution:

$$\mu_{ex} = \mu^0_{ex} + (g_H + g_{XC})n_{ex} + g_H n_S \tag{9}$$

where $n_S = n_D$ are the equal densities of electrons and holes in the two electrodes. Eq. (9) can be obtained by minimizing the total energy, $\mathcal{E}[n_S, n_{ex}]$, with respect to n_{ex} (see Supplemental Material [42]). By minimizing $\mathcal{E}[n_S, n_{ex}]$ with respect to n_S we obtain the following expression for the bias potential,

$$\frac{n_{ex}}{C_{DL}} + n_S\left(\frac{2\hbar v\sqrt{2\pi}}{e^2\sqrt{|n_S|}} + \frac{1}{C_{geo}}\right) = \frac{V_b}{e}. \tag{10}$$

In Eq. (10), $C_{geo} = \epsilon/(4\pi e^2 d_{tot})$ is the geometric capacitance and $d_{tot} = d_S + d_{DL} + d_D$; the energy function used to derive Eq. (10) does not account for exchange and correlation in the electrodes, *i.e.* for interaction corrections to the electrode quantum capacitance, but these can easily be added when relevant. A time-independent equilibrium between the electrodes and the exciton fluid is established when $n_{ex} \neq 0$ and electron-hole pairs have the same chemical potential in either environment *i.e.* when and $eV_b = \mu_{ex}$.

Fig. 3 shows equilibrium densities calculated for several typical values of the dimensionless exchange-correlation coupling strength $\beta \equiv g_{XC}/g_H$. Below we take β as an unknown parameter and show that its value can be measured electrically. When estimated using self-consistent mean-field theory β changes sign from positive to negative when d_{DL} exceeds around a quarter of an excitonic Bohr radius, and using TMD semiconductor parameters has the value $\beta = -0.6$ for $d_{DL} = 1$nm in [41]. Below the threshold voltage $V_{\rm th}$, which satisfies $eV_{\rm th} = \mu^0_{ex} + g_H n_S(V_{\rm th})$ and depends on d_S/d_{DL}, no excitons are injected and $n_S(V_b)$ is independent of β, as shown in Fig. 3(a). When $V_b > V_{\rm th}$, electrons and holes can enter the TMD layers by forming excitons via the two-particle tunneling process. The slope of the $n_S(V_b)$ curve is reduced and becomes negative when β changes sign from positive to negative. For $\beta < 0$, we find that n_S becomes negative when $V_b = -\mu^0_{ex}/\beta$; we show later that the dynamic response is anomalous at this point.

The two-particle tunneling rate which we have estimated theoretically can be measured by performing *ac* electrical measurements, letting $V_b(t) = V_{dc} + V_{ac}\cos\omega t$, where V_{ac} is small. The linear response of the system to V_{ac} can be extracted by linearizing Eq. (7) and (10) (see details in Supplemental Material [42]). In Fig. 4 we plot normalized amplitudes of the differential conductance $|dI/dV|/\bar{G}_{ex}$, where $\bar{G}_{ex}(V_{dc})$ is the *dc* exciton conductance G_{ex}. In the low and high frequency limits, the system behaves effectively as a capacitor with $C^{eff}_{low} = a_0 C_{DL}$, $C^{eff}_{high} = a_\infty C_{DL}$, where $\gamma = (1 + 2C_{geo}/C_Q)d_{tot}/d_{DL}$ and $a_0 = \{(\gamma-1)^2/[(1+\beta)\gamma-1]+1\}/\gamma$ and $a_\infty = 1/\gamma$. $C_Q = \sqrt{2n_S}/(\sqrt{\pi}\hbar v)$ is the quantum capacitance of graphene [43]. dI/dV deviates from linear frequency dependence when the scaled frequency $x = \omega C_{DL}/\bar{G}_{ex} \sim x_0 = [(1+\beta)\gamma-1]/\gamma$. Measuring the crossover frequency ω_0, gives the tunneling conductance $\bar{G}_{ex} = \omega_0 C_{DL}/x_0$. The *dc* bias voltage dependence of the differential conductance is shown in Fig. 4(b). For $\beta < 0$ a peak appears at $V_{\rm peak} = -E^0_{ex}/\beta$, the point at which n_S reaches 0, as mentioned above. This suggests a way to measure the exciton exchange-correlation energy parameter g_{XC}, provided that E_g and E_b are known. For $\beta > 0$, the differential conductance increases slowly with increasing V_b in the regime $V_b > V_{\rm th}$.

Optical recombination, which provides a mechanism for excitons to leak out of the system of interest, can easily be added to the theory explained here, and in the dc bias voltage case converts the equilibrium exciton fluid into a steady state. When the steady state exciton fluid condenses, it will emit coherent light forming a state similar to a polariton laser but subject to precise electrical control.

This work was supported by the Army Research Office under Award W911NF-17-1-0312 and by the Welch

Foundation under grant TBF1473. Ming Xie was supported by The Center for Dynamics and Control of Materials (CDCM) under NSF Award DMR-1720595. The authors acknowledge helpful discussions with Hui Deng, Jim Eisenstein, Emanuel Tutuc, and David Snoke.

[1] Y. Lozovik and V. Yudson, JETP Lett. **22**, 274 (1976).
[2] L. V. Keldysh and A. N. Kozlov, Sov. Phys. JETP **27**, 521 (1968).
[3] L. V. Butov, A. L. Ivanov, A. Imamoglu, P. B. Littlewood, A. A. Shashkin, V. T. Dolgopolov, K. L. Campman, and A. C. Gossard, Phys. Rev. Lett. **86**, 5608 (2001).
[4] L. V. Butov, C. W. Lai, A. L. Ivanov, A. C. Gossard, and D. S. Chemla, Nature **417**, 47 (2002).
[5] A. V. Gorbunov and V. B. Timofeev, JETP Lett. **83**, 146 (2006).
[6] A. A. High, J. R. Leonard, A. T. Hammack, M. M. Fogler, L. V. Butov, A. V. Kavokin, K. L. Campman, and A. C. Gossard, Nature **483**, 584 (2012).
[7] A. A. High, J. R. Leonard, M. Remeika, L. V. Butov, M. Hanson, and A. C. Gossard, Nano Lett. **12**, 2605 (2012).
[8] H. Deng, G. Weihs, C. Santori, J. Bloch, and Y. Yamamoto, Science **298**, 199 (2002).
[9] J. Kasprzak, M. Richard, S. Kundermann, A. Baas, P. Jeambrun, J. M. J. Keeling, F. M. Marchetti, M. H. Szymanska, R. Andre, J. L. Staehli, V. Savona, P. B. Littlewood, B. Deveaud, and L. S. Dang, Nature **443**, 409 (2006).
[10] R. Balili, V. Hartwell, D. Snoke, L. Pfeiffer, and K. West, Science **316**, 1007 (2007).
[11] J. J. Baumberg, A. V. Kavokin, S. Christopoulos, A. J. D. Grundy, R. Butté, G. Christmann, D. D. Solnyshkov, G. Malpuech, G. Baldassarri Höger von Högersthal, E. Feltin, J.-F. Carlin, and N. Grandjean, Phys. Rev. Lett. **101**, 136409 (2008).
[12] E. Wertz, L. Ferrier, D. D. Solnyshkov, R. Johne, D. Sanvitto, A. Lemaitre, I. Sagnes, R. Grousson, A. V. Kavokin, P. Senellart, G. Malpuech, and J. Bloch, Nat Phys **6**, 860 (2010).
[13] D. Snoke, Science **298**, 1368 (2002).
[14] H. Deng, H. Haug, and Y. Yamamoto, Rev. Mod. Phys. **82**, 1489 (2010).
[15] I. Carusotto and C. Ciuti, Rev. Mod. Phys. **85**, 299 (2013).
[16] T. Byrnes, N. Y. Kim, and Y. Yamamoto, Nat Phys **10**, 803 (2014).
[17] D. Sanvitto and S. Kena-Cohen, Nat Mater **15**, 1061 (2016).
[18] Y. Sun, P. Wen, Y. Yoon, G. Liu, M. Steger, L. N. Pfeiffer, K. West, D. W. Snoke, and K. A. Nelson, Phys. Rev. Lett. **118**, 016602 (2017).
[19] C. Schneider, A. Rahimi-Iman, N. Y. Kim, J. Fischer, I. G. Savenko, M. Amthor, M. Lermer, A. Wolf, L. Worschech, V. D. Kulakovskii, I. A. Shelykh, M. Kamp, S. Reitzenstein, A. Forchel, Y. Yamamoto, and S. Hofling, Nature **497**, 348 (2013).
[20] P. Bhattacharya, B. Xiao, A. Das, S. Bhowmick, and J. Heo, Phys. Rev. Lett. **110**, 206403 (2013).
[21] P. Bhattacharya, T. Frost, S. Deshpande, M. Z. Baten, A. Hazari, and A. Das, Phys. Rev. Lett. **112**, 236802 (2014).
[22] Y. Yao, A. J. Hoffman, and C. F. Gmachl, Nat. Photonics **6**, 432 (2012).
[23] For systems in which dark excitons (excitons with momentum or spin quantum numbers that don't match those of the photons) are favored however, direct optical access is blocked.
[24] K. Cohen, Y. Shilo, K. West, L. Pfeiffer, and R. Rapaport, Nano Lett. **16**, 3726 (2016).
[25] Y. Shilo, K. Cohen, B. Laikhtman, K. West, L. Pfeiffer, and R. Rapaport, Nat. Comm. **4**, 2335 EP (2013).
[26] D. Y. Qiu, F. H. da Jornada, and S. G. Louie, Phys. Rev. Lett. **111**, 216805 (2013).
[27] K. F. Mak, K. He, C. Lee, G. H. Lee, J. Hone, T. F. Heinz, and J. Shan, Nat. Mater. **12**, 207 (2013).
[28] M. M. Fogler, L. V. Butov, and K. S. Novoselov, Nat. Comm. **5**, 4555 EP (2014).
[29] A. K. Geim and I. V. Grigorieva, Nature **499**, 419 (2013).
[30] K. S. Novoselov, A. Mishchenko, A. Carvalho, and A. H. Castro Neto, Science **353**, aac9439 (2016).
[31] K. F. Mak and J. Shan, Nat. Photonics **10**, 216 (2016).
[32] P. Rivera, J. R. Schaibley, A. M. Jones, J. S. Ross, S. Wu, G. Aivazian, P. Klement, K. Seyler, G. Clark, N. J. Ghimire, J. Yan, D. G. Mandrus, W. Yao, and X. Xu, Nat. Commun. **6**, 6242 (2015).
[33] M. Palummo, M. Bernardi, and J. C. Grossman, Nano Lett. **15**, 2794 (2015).
[34] E. V. Calman, M. M. Fogler, L. V. Butov, S. Hu, A. Mishchenko, and A. K. Geim, arXiv:1709.07043.
[35] A. Raja, A. Chaves, J. Yu, G. Arefe, H. M. Hill, A. F. Rigosi, T. C. Berkelbach, P. Nagler, C. Schüller, T. Korn, C. Nuckolls, J. Hone, L. E. Brus, T. F. Heinz, D. R. Reichman, and A. Chernikov, Nat. Comm. **8**, 15251 EP (2017).
[36] C. Zhang, C. Gong, Y. Nie, K.-A. Min, C. Liang, Y. J. Oh, H. Zhang, W. Wang, S. Hong, L. Colombo, R. M. Wallace, and K. Cho, 2D Materials **4**, 015026 (2017).
[37] R. Bistritzer and A. H. MacDonald, Phys. Rev. B **81**, 245412 (2010).
[38] K. Zhou, D. Wickramaratne, S. Ge, S. Su, A. De, and R. K. Lake, Phys. Chem. Chem. Phys. **19**, 10406 (2017).
[39] C. Comte and P. Nozires, J. Phys. France **43**, 1069 (1982).
[40] X. Zhu, P. B. Littlewood, M. S. Hybertsen, and T. M. Rice, Phys. Rev. Lett. **74**, 1633 (1995).
[41] F.-C. Wu, F. Xue, and A. H. MacDonald, Phys. Rev. B **92**, 165121 (2015).
[42] See Supplemental Material for the discussion of the total energy functional $\mathcal{E}[n_S, n_{ex}]$, the existence of a global minimum and a detailed derivation of the *ac* response equations.
[43] J. Xia, F. Chen, J. Li, and N. Tao, Nat. Nanotechnol. **4**, 505 (2009).